

# Towards Facilitated Fairness Assessment of AI-based Skin Lesion Classifiers Through GenAI-based Image Synthesis

Ko Watanabe\*

DFKI GmbH  
ko.watanabe@dfki.de

Stanislav Frolov\*

DFKI GmbH  
stanislav.frolov@dfki.de

Aya Hassan

RPTU Kaiserslautern-Landau  
aya.hassan@dfki.de

David Dembinsky

DFKI GmbH  
david.dembinsky@dfki.de

Adriano Lucieri

DFKI GmbH  
adriano.lucieri@dfki.de

Andreas Dengel

DFKI GmbH  
andreas.dengel@dfki.de

\*Equal contribution

## Abstract

Recent advances in deep learning and on-device inference could transform routine screening for skin cancers. Along with the anticipated benefits of this technology, potential dangers arise from unforeseen and inherent biases. A significant obstacle is building evaluation datasets that accurately reflect key demographics, including sex, age, and race, as well as other underrepresented groups. To address this, we train a state-of-the-art generative model to generate synthetic data in a controllable manner to assess the fairness of publicly available skin cancer classifiers. To evaluate whether synthetic images can be used as a fairness testing dataset, we prepare a real-image dataset (MILK10K) as a benchmark and compare the True Positive Rate result of three models (DeepGuide, MelaNet, and SkinLesionDensnet). As a result, the classification tendencies observed in each model when tested on real and generated images showed similar patterns across different attribute data sets. We confirm that highly realistic synthetic images facilitate model fairness verification.

## 1. Introduction

Melanoma is the deadliest form of skin cancer, with an estimated 325,000 new cases (174,000 men and 151,000 women) and 57,000 deaths (32,000 men and 25,000 women) reported worldwide in 2020 [3]. By 2040, incidence is projected to increase by nearly 50% to 510,000 new cases, and mortality by 68% to 96,000 deaths. Early detection, however, dramatically improves survival. For example, a population-wide screening project in Schleswig-Holstein, Germany, reported a reduction in melanoma mortality of 47% for men and 49% for women

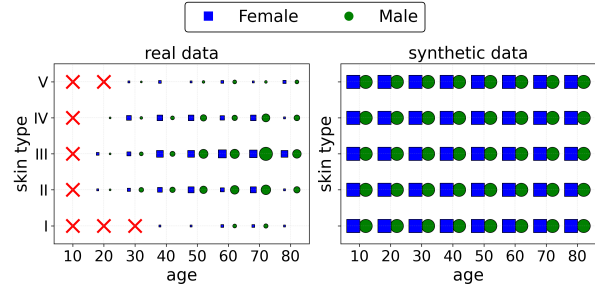


Figure 1. Real melanoma test data (left) such as MILK10k [36] shows limited and imbalanced demographic coverage, while synthetic data (right) can provide complete combinations with balanced sampling, enabling more reliable fairness assessment.

[26]. Similarly, screening efforts in Australia decreased melanoma deaths by 59% [58]. These findings underline a crucial insight: despite rising incidence, early and accessible screening can substantially reduce mortality.

Recent advances in Artificial Intelligence (AI), together with the widespread availability of high-resolution smartphone cameras, have created new opportunities for accessible melanoma pre-screening outside clinical environments. AI-assisted diagnostic systems can support clinicians during routine examinations and also provide human-understandable explanations for their decisions [33]. In principle, such systems could even enable remote pre-screening, allowing individuals to capture dermoscopic images themselves and receive preliminary risk assessments [9, 45]. These innovations have considerable societal potential, including earlier detection, reduced diagnostic delays, lower healthcare costs, and decreased clinician workload.

At the same time, the deployment of AI in medicine requires a high level of trustworthiness, especially in light

of regulatory developments such as the EU AI Act [14]. Fairness and transparency in both datasets and trained models are essential conditions for reliable clinical use [1, 2, 5, 6, 12, 39]. Fairness assessments depend on access to demographically well-characterized data. The International Skin Imaging Collaboration (ISIC) archive [18] provides one of the most comprehensive publicly available skin lesion datasets [10, 11, 18, 21, 48, 56], including metadata such as sex, age, and Fitzpatrick skin type [51]. Despite its scale and quality, demographic imbalance remains a major limitation and complicates fairness evaluations.

Meanwhile, recent progress in Generative AI (GenAI), particularly diffusion models [22, 47], has enabled high-fidelity and attribute-controlled image synthesis. In this work, we explore whether these advances can support fairness evaluation in melanoma detection. Using the ISIC dataset and LightningDiT [59], a latent diffusion transformer [41], we train a generative model capable of synthesizing realistic dermoscopic images conditioned on key patient attributes. We then examine whether such synthetic cohorts can serve as a reliable resource for assessing algorithmic fairness in publicly available melanoma classifiers. In summary, our work makes the following key contributions.

- We present a diffusion-based framework for generating demographically balanced cohorts of dermoscopic images. Our model synthesizes high-fidelity skin lesion images conditioned on sex, age, and Fitzpatrick skin type.
- We introduce a protocol for fairness evaluation that applies the generated images to three peer-reviewed melanoma classifiers and quantifies true positive rate disparity.
- We provide an empirical analysis of the suitability of synthetic, demographically balanced cohorts for fairness auditing and discuss implications for future medical AI evaluation workflows.

## 2. Related Work

The following sections review related work in three areas: generative models for synthetic data generation, melanoma detection models, and fairness evaluation in skin lesion classification.

### 2.1. Generative Models for Skin Lesions

Synthetic data generation is widely used to address data scarcity, class imbalance, and privacy concerns in skin lesion datasets. Early approaches based on Generative Adversarial Networks (GANs) [17], such as MelanoGANs [4], DCGAN [43], and LAPGAN [13], demonstrated that realistic dermoscopic images can be synthesized even from limited data. DermGAN [16] and StyleGAN-

based methods [7, 24] introduced finer control over lesion characteristics and improved downstream classifier performance. Later work, including StyleGAN2 [25] and federated setups [8], further improved stability, fidelity, and privacy. Diffusion models now dominate high-fidelity medical image synthesis. Stable Diffusion [47] and DreamBooth [49], as applied in Cancer-Net SCA-Synth [54], support few-shot personalization and balanced dataset construction. Extensions of latent diffusion models have also improved control over skin type variation and helped address fairness gaps [57]. Our work differs by focusing on fairness evaluation rather than augmentation. We train a state-of-the-art latent diffusion transformer based on LightningDiT [59] to generate attribute-controlled dermoscopic image cohorts. The model leverages all available ISIC metadata and allows systematic control over demographic and clinical attributes for constructing balanced intersectional test sets.

### 2.2. Melanoma Detection Models

Prior research on melanoma classification has employed a variety of datasets, including ISIC, Derm7pt [27], and HAM [56], the latter containing 10,015 dermoscopic images covering seven lesion types. These datasets differ in composition, imaging style, and demographic distribution, which complicates direct model comparison. A further challenge arises from the heterogeneous evaluation metrics reported in the literature. Some studies rely on the F1-score, whereas others report AUC or AUROC, making cross-model comparison nontrivial. Pretrained model availability also varies. Public weights exist for DeepGuide [35], MelaNet [61], and SkinLesionDensenet [40], but not for Patch-Lesion [15] or EFFNet [34]. In this work, we use publicly available pretrained models to ensure reproducibility and consistent evaluation.

### 2.3. Fairness in Skin Lesion Classification

Fairness evaluation has gained increasing attention due to persistent performance disparities across demographic subgroups. In [2], the authors proposed an augmentation strategy that combines a source skin tone image with a diagnostic image to mitigate imbalance and skin tone bias. Other approaches incorporate fairness directly into model design. BiaslessNAS [52] integrates fairness constraints throughout the neural architecture search process and reports improvements of 2.55% in accuracy and 65.50% in fairness over baseline models. Compared to previous augmentation-based fairness approaches, our method generates attribute-controlled synthetic images through text prompts. We evaluate fairness in existing pretrained melanoma classifiers [35, 40, 61] using balanced synthetic cohorts, allowing us to investigate the potential of prompt-driven generative models as a tool

| Model                     | Architecture    | Dataset   | Public Weights | Performance      |
|---------------------------|-----------------|-----------|----------------|------------------|
| DeepGuide ([35])          | DenseNet        | Derm7pt   | ✓              | 0.788 (AUC)      |
| MelaNet ([61])            | VGG-GAP         | ISIC 2016 | ✓              | 0.811 (AUROC)    |
| Patch-Lesion ([15])       | Dense121        | HAM10000  | –              | 0.855 (F1-Score) |
| SkinLesionDensenet ([40]) | DenseNet201     | ISIC      | ✓              | 0.878 (F1-Score) |
| EFFNet ([34])             | EfficientNetV2  | HAM10000  | –              | 0.932 (F1-Score) |
| Sabir and Mehmood [50]    | EfficientNet-B0 | HAM10000  | –              | 0.970 (F1-Score) |

Table 1. Comparison of existing melanoma detection models.

for systematic fairness assessment.

### 3. Methodology

In this section, we first describe the process for generating synthetic test data. Next, we describe the fairness evaluation process against the selected pre-trained models for melanoma detection. In Figure 2, we illustrate our complete fairness testing workflow.

#### 3.1. Synthetic Test Data Generation

**Model:** Our fairness evaluation relies on a controllable generative model capable of producing high-fidelity dermoscopic images across clinically and demographically relevant attributes. We train a latent diffusion transformer using the LightningDiT framework [59]. LightningDiT improves reconstruction and generative quality by aligning the underlying variational autoencoder (VAE) [28] with pretrained vision foundation models. The resulting vision foundation model aligned VAE (VA-VAE) produces latent representations that are consistent with models such as DINOv2 [38] and MAE [20], which enhances semantic structure and supports reliable attribute conditioning. The latent diffusion transformer contains 675M parameters and is trained for 80,000 steps using AdamW [32], a learning rate of 0.0002, mixed precision, and a global batch size of 1024 on 8×A100 GPUs. Training requires approximately 8 hours.

**Data:** Only publicly available data are used and no new patient information is collected. All dermoscopic images from the ISIC archive (2016–2024) are processed at a resolution of  $256 \times 256$  and encoded into the latent space using the VA-VAE, resulting in roughly 500,000 latent-image pairs. Each image is paired with a text description constructed from the available annotations, including sex, age group, lesion size, Fitzpatrick skin type, and diagnosis. Data with insufficient attributes are excluded. Text embeddings are produced using CLIP [44], a contrastively trained vision-language model that embeds images and text into a shared latent space and provides strong semantic grounding for conditioning.

**Generation:** After training, the model acts as a controllable generator for constructing balanced synthetic test sets. Synthetic dermoscopic images are produced by sam-

pling random latent noise and conditioning the model on attribute-specific text prompts that target demographic groups under evaluation. We use the Euler solver with 400 diffusion steps and a classifier-free guidance scale of 4. The resulting images form consistent, attribute-controlled cohorts for downstream fairness assessment.

#### 3.2. Balanced Test Data Generation

**Overview:** To evaluate fairness in melanoma classification models, we create a synthetic test set that is explicitly balanced across relevant Personal Identifiable Information (PII) attributes. As illustrated in Figure 2, images are generated through a systematic prompting procedure applied to our trained generative model. Each prompt specifies the demographic attributes of interest while other visual factors are held as consistent as possible. This controlled setup reduces confounding variation and ensures that differences in classifier predictions can be traced to subgroup-specific effects rather than distributional imbalance.

**Prompt Design:** We adopt a full-factorial scheme across four PII dimensions: sex (2 categories), age group (8 categories), Fitzpatrick skin type (6 categories), and disease case (1 category corresponding to melanoma). This yields 96 unique attribute configurations ( $2 \times 8 \times 6 \times 1$ ), covering key demographic and phenotypic factors known to influence dermatological diagnosis.

**Sampling Strategy:** For each configuration, we generate 850 synthetic melanoma images to ensure equal subgroup representation. The resulting test set contains 81,600 images and provides a balanced distribution across all selected PII factors. This design enables a controlled and statistically robust assessment of fairness in pretrained melanoma classification models.

#### 3.3. Fairness Assessment

**Metric Definition:** Since our synthetic test set contains only melanoma (*i.e.* positive) cases, we quantify subgroup disparities using TPR disparity [19], defined as the difference between the maximum and minimum true positive rates across PII groups. In a positive-only setting, the proportion of predicted positives in each group coincides with sensitivity. For a single decision threshold  $\tau$

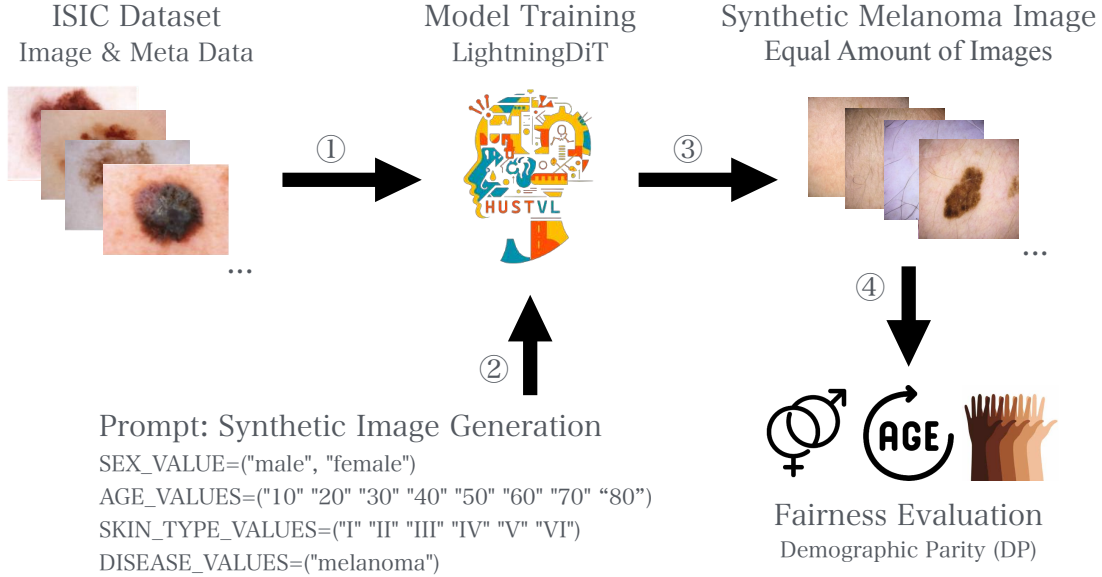


Figure 2. Overall pipeline of our fairness testing workflow. We first train a generative model based on LightningDiT [59] using the ISIC dataset. Synthetic melanoma test images are then generated via systematic prompt templates. Finally, the synthetic images are used to assess fairness as measured via True Positive Rate (TPR) difference in pre-trained melanoma detection models.

shared across all groups:

$$\text{TPR}(g) = \frac{1}{|D_g^+|} \sum_{(x,y) \in D_g^+} \mathbf{1}\{\hat{f}(x) \geq \tau\}, \quad (1)$$

$$\Delta_{\text{TPR}} = \max_g \text{TPR}(g) - \min_g \text{TPR}(g) \quad (2)$$

We compute  $\Delta_{\text{TPR}}$  on synthetic cohorts stratified by sex, age group, and Fitzpatrick skin type. To generate a strictly positive-only test set, we use “melanoma” as the disease value in our systematic prompt configuration. The resulting measure,  $\Delta_{\text{TPR}}$ , therefore provides a meaningful and statistically robust indicator of whether a model systematically favors or disadvantages particular demographic groups [29, 31, 53].

**Evaluation Protocol:** The balanced and fully factorial nature of the synthetic test set enables unbiased comparisons across demographic subgroups. Although the dataset contains only positive cases for computing TPR, it can also be used for additional performance metrics whose thresholds are determined externally, such as sensitivity, specificity, and AUROC. This setup supports both macro-averaged and worst-case subgroup analysis, and thus provides a rigorous basis for evaluating fairness in melanoma classification models.

**Models:** We evaluate three publicly available pretrained melanoma classifiers: DeepGuide [35], MelaNet [61], and SkinLesionDensenet [40]. These models were selected due to the availability of pretrained weights and their relevance in prior benchmark studies. *MelaNet*

and *SkinLesionDensenet* are trained on ISIC, whereas *DeepGuide* is trained on the HAM10000 (HAM) dataset, providing complementary training distributions. Architecturally, *DeepGuide* and *SkinLesionDensenet* rely on DenseNet backbones, while *MelaNet* is based on a VGG-GAP design. This diversity in both training data and network architecture offers a representative foundation for examining fairness behavior across classifier families.

## 4. Results and Discussion

### 4.1. Generated Synthetic Skin Lesion Images

Figure 3 presents representative melanoma images synthesized by our model under controlled prompting. The vertical axis enumerates Fitzpatrick skin types (I–VI) for each sex (male and female), while the horizontal axis spans age categories in 10-year increments from 10 to 80 years. This grid structure facilitates visual inspection of demographic variation. The generator responds to conditioning in a largely coherent manner, with clear subgroup-specific differences in appearance.

While the generated images are highly realistic, one limitation is immediately noticeable. The generated images do not become increasingly darker with higher Fitzpatrick skin type. For example, the generated images do not become progressively darker with higher Fitzpatrick skin types. Although this might be the intuitive expectation, prior work [23, 55] shows that lighting, camera settings, and lesion visibility introduce substantial variability, making pixel intensity an unreliable indicator.

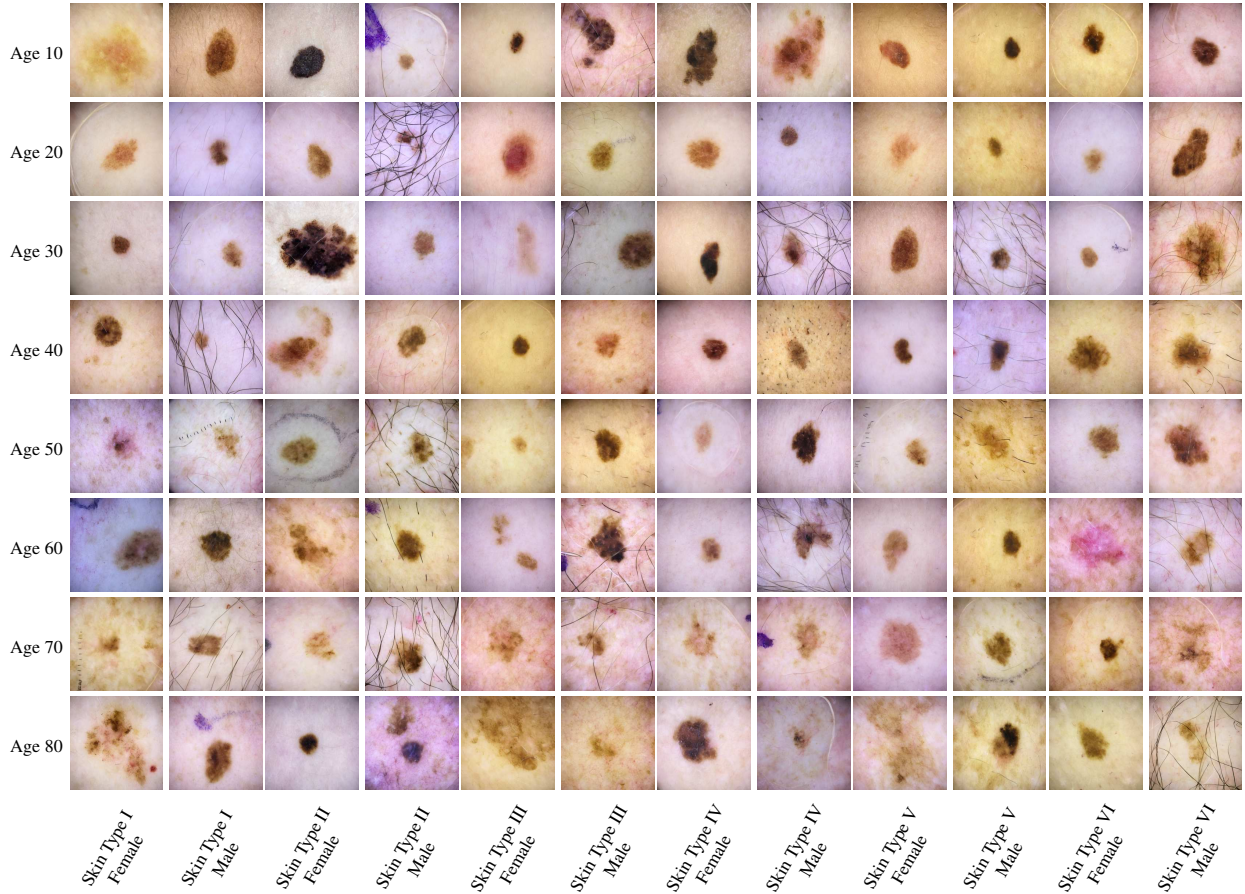


Figure 3. Synthetic melanoma images generated by our model. Rows represent Fitzpatrick skin types (I–VI) combined with sex, and columns represent age groups (10–80). The grid demonstrates coverage of diverse demographic groups for fairness assessment.

Further details and visual comparisons with real data exhibiting the same issue are provided in the appendix.

Given that downstream fairness analysis relies critically on the quality and diversity of the synthetic images, principled quality-control procedures are essential. Section 5.2 discusses possible approaches, including attribute-specific judging models and screening using vision–language models prior to classifier evaluation. Such methods are intended to detect unrealistic or low-diversity generations before they influence fairness conclusions.

## 4.2. Evaluation of Fairness Performance

**Group-wise TPR on Real and Synthetic Cohorts:** Figure 4 summarizes group-wise fairness results for the three pretrained melanoma classifiers across sex, age group, and Fitzpatrick skin type. Since the synthetic test set contains only melanoma (positive) cases, the melanoma prediction rate shown in the figure corresponds directly to sensitivity. To compare real and synthetic testing, we compute the performance on MILK4K and on the syn-

thetic cohort separately. Following Section 3.3, we apply a single shared decision threshold and quantify disparity as the difference between the maximum and minimum TPR values within each attribute. Overall, real and synthetic image testing exhibit similar trends. When sex is treated as the target attribute, both *DeepGuide* and *MelaNet* achieve higher accuracy for male than for female, whereas with the same test images *SkinLesionDensenet* performs better for female than for male. This demonstrates that synthetic data can reproduce the gender bias observed on real-world data. For age, *MelaNet* shows that older age groups are associated with higher TPR for both MILK4K and synthetic images, indicating that age-related biases are also reflected in the synthetic cohort. For skin type, the performance ranking of *MelaNet*, *SkinLesionDensenet*, and *DeepGuide* is consistent between real and synthetic testing. A plausible explanation for the skin-type trends is a distributional shift between training and test data. Both *MelaNet* and *SkinLesionDensenet* are trained on ISIC, whereas *DeepGuide*

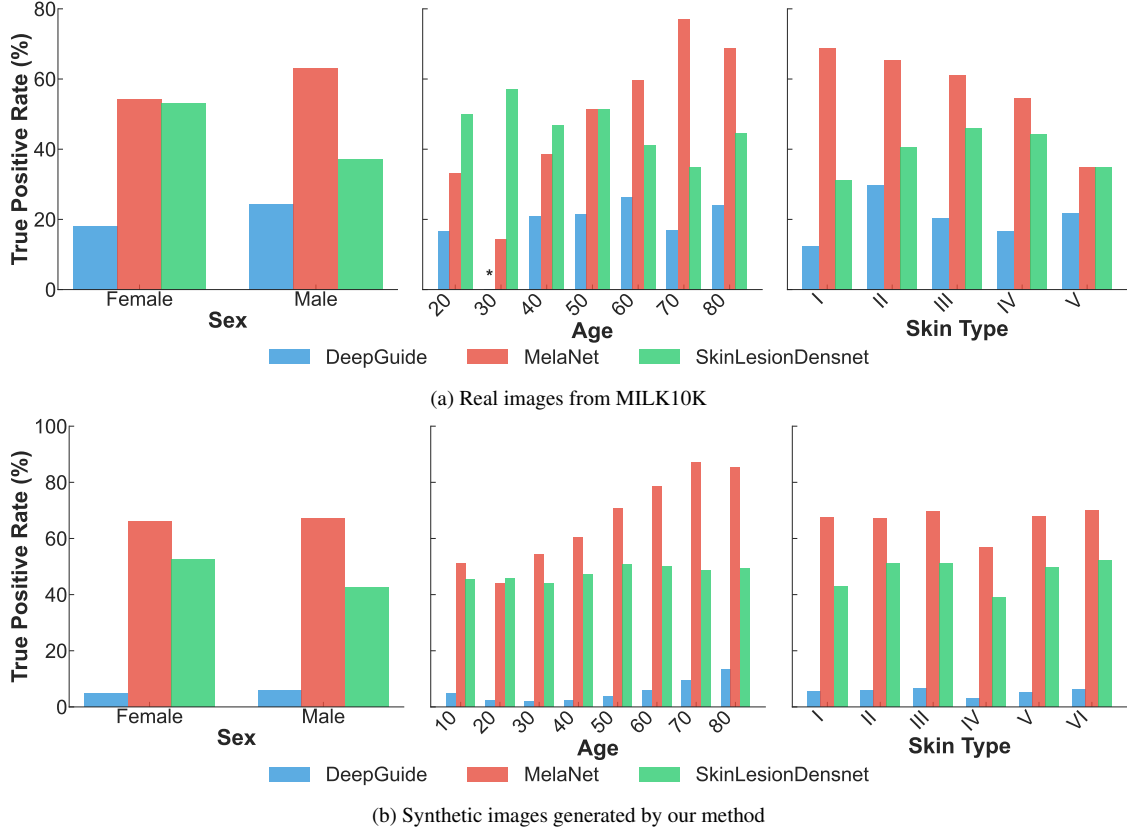


Figure 4. TPR of the skin lesion classifier across different PII (sex, age, and Fitzpatrick skin type) groups. The result present that both real and synthetic image testing perform a similar bias trend for each *DeepGuide*, *MelaNet*, and *SkinLesionDensnet*.

is trained on the HAM dataset. Because the training and test sources differ, similar relative performance patterns emerge across both real and synthetic image testing.

**Effect of Test Set Size:** Figure 5 shows cumulative TPR as a function of the number of test images. The data count corresponds to the number of images used and illustrates how recognition accuracy changes as more test data are included. As a rule of thumb, as the number of test images increases, convergence to a stable accuracy is expected [46]. Therefore, if accuracy trends for real and synthetic images converge, fairness simulations can be reliably performed using generated images. For sex, both male and female curves exhibit this convergence behavior, and synthetic testing closely tracks real-image performance as the available data volume increases. In contrast, the age-related curves for real and synthetic data do not fully converge, suggesting that the generator and real data distributions differ more strongly along the age dimension. Age is a factor with substantial intra-group variability (e.g., early versus late decades), which may contribute to these discrepancies and should be examined in future work.

**Attribute-wise TPR Disparities:** Table 2 reports the

maximum, minimum, and range of TPR across subgroups for each attribute. For sex and skin type, *MelaNet* achieves both the highest overall performance and the smallest disparity  $\Delta_{\text{TPR}}$ . On the synthetic cohort,  $\Delta_{\text{TPR}}$  for sex is 0.0115 and for Fitzpatrick skin type is 0.1322. Interestingly, for the age attribute, *MelaNet* exhibits the largest disparity, whereas *SkinLesionDensnet* is substantially fairer: its  $\Delta_{\text{TPR}}$  for age is 0.0682, the lowest among the three models. These patterns are consistent between real and synthetic testing, reinforcing the usefulness of the synthetic cohort for fairness comparison.

**Methodological Implications:** These results illustrate two methodological advantages of our approach. First, attribute-conditioned synthetic data enable direct, fine-grained comparisons of subgroup sensitivities within a controlled, fully balanced design. Second, by training generators on different data sources, fairness analysis can be extended to examine the influence of the training data itself. In practice, we recommend a two-step protocol: (i) verify that a pretrained model achieves reasonable sensitivity on synthetic images that match its training distribution, and only then (ii) assess subgroup disparities. This procedure yields more reliable conclusions

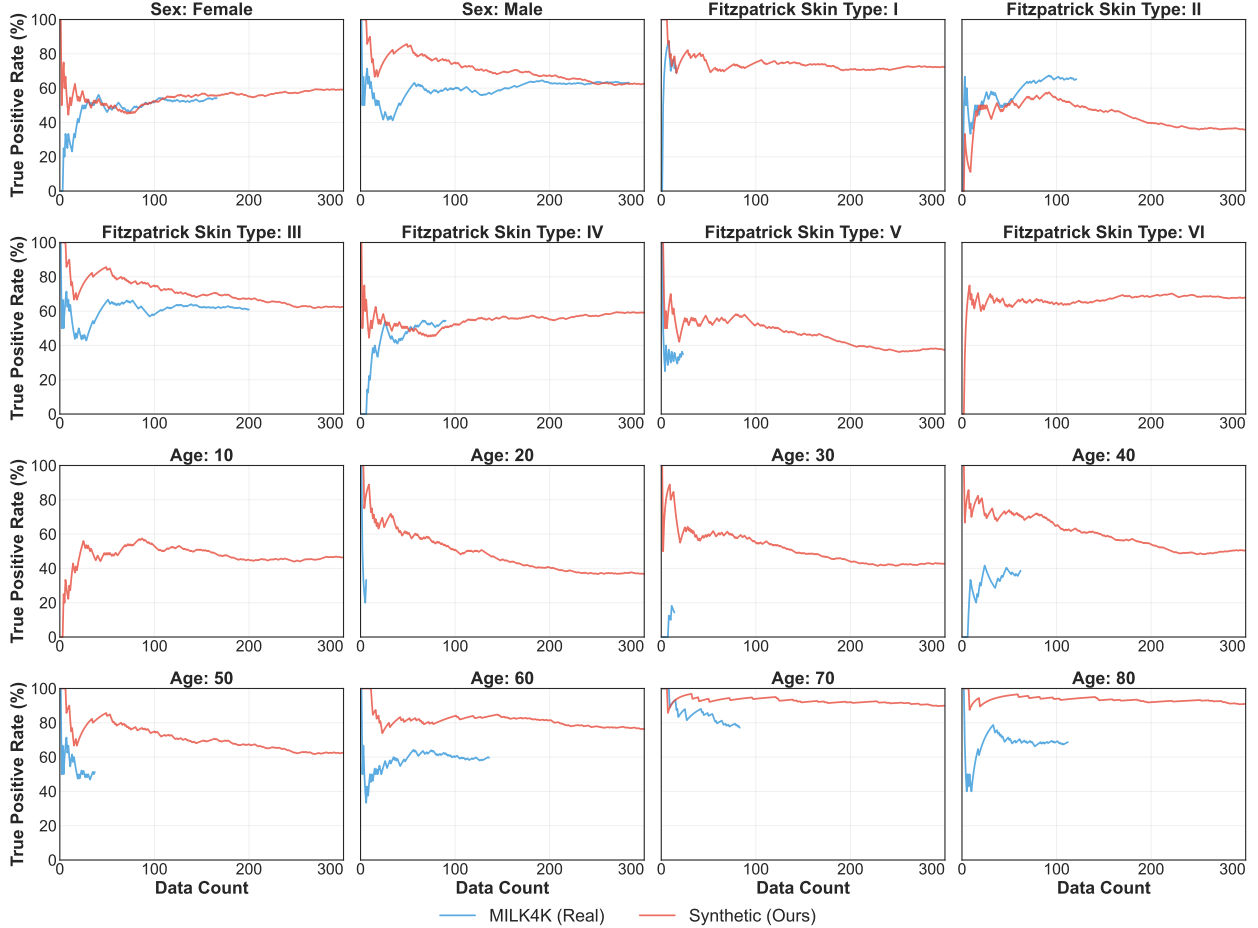


Figure 5. Cumulative TPR curves for the PII attributes on MILK10K (real) and our synthetic images using MelaNet. The results show that the TPR converges to similar levels, particularly for sex and skin type, indicating that synthetic images can serve as a suitable fairness evaluation dataset.

| Model              | Dataset | Sex        |            |                                  | Age         |             |                                  | Fitzpatrick Skin Type |             |                                  |
|--------------------|---------|------------|------------|----------------------------------|-------------|-------------|----------------------------------|-----------------------|-------------|----------------------------------|
|                    |         | Max        | Min        | $\Delta_{\text{TPR}} \downarrow$ | Max         | Min         | $\Delta_{\text{TPR}} \downarrow$ | Max                   | Min         | $\Delta_{\text{TPR}} \downarrow$ |
| DeepGuide          | Ours    | 0.0601 (M) | 0.0487 (F) | 0.0114                           | 0.1337 (80) | 0.0189 (30) | 0.1148                           | 0.0643 (III)          | 0.0311 (IV) | 0.0332                           |
|                    | MILK4K  | 0.2430 (M) | 0.1807 (F) | 0.0622                           | 0.2647 (60) | 0.1667 (20) | 0.0980                           | 0.2975 (II)           | 0.1250 (I)  | 0.1725                           |
| MelaNet            | Ours    | 0.6706 (M) | 0.6591 (F) | 0.0115                           | 0.8693 (70) | 0.4404 (20) | 0.4289                           | 0.7004 (VI)           | 0.5682 (IV) | 0.1322                           |
|                    | MILK4K  | 0.6303 (M) | 0.5422 (F) | 0.0881                           | 0.7711 (70) | 0.1429 (30) | 0.6282                           | 0.6875 (I)            | 0.3478 (V)  | 0.3397                           |
| SkinLesionDensenet | Ours    | 0.5255 (F) | 0.4267 (M) | 0.0988                           | 0.5081 (50) | 0.4399 (30) | 0.0682                           | 0.5209 (VI)           | 0.3899 (IV) | 0.1310                           |
|                    | MILK4K  | 0.5301 (F) | 0.3732 (M) | 0.1569                           | 0.5714 (30) | 0.3494 (70) | 0.2220                           | 0.4600 (III)          | 0.3125 (I)  | 0.1475                           |

Table 2. Performance comparison of maximum (Max) TPR, minimum (Min) TPR, and TPR difference ( $\Delta_{\text{TPR}}$ ) across attributes (Sex, Age, Skin Type). The symbol next to the value indicates which attribute it corresponds to, such as M is Male and F is Female.

regarding model fairness and highlights the importance of dataset-model alignment in fairness evaluations.

## 5. Limitations and Future Work

In the following, we discuss limitations and future research directions.

### 5.1. Enhancing Dataset Use for Training

In this work, we generated synthetic image test data by training a custom LightningDiT [59]. According to Figure 3, the images show high realism, and Figure 5 confirms a similar trend in the cumulative TPR comparison between real and synthetic images. However, according

to Figure 5, age TPR conversion differs between real and synthetic images. This may be due to the training procedure, which determines the precision of the label used for training. The next step to improve the synthetic image generation model is to include a detail attribute in the training procedure of our generative model. Another direction is to add multiple datasets and use different image capturing devices to make the dataset and thus generation process more robust.

## 5.2. Quality Control of the Synthetic Images

In our work, we evaluate fairness performance through 81,600 synthetic images generated in a pattern presented in Section 3.2. To ensure the quality of the generated images, further quality control models could be used that evaluate the reliability of the images [30]. The approach may, for example, be to implement quality-judging models for each age, sex, and skin color. Also, due to the significant recent growth of visual language models (VLMs) [60], VLM-as-a-judge may be an approach to perform quality evaluation before model prediction. Hence, the next step in the current architecture is also to consider new models for quality assurance of the test images.

## 5.3. Understanding Causes of Unfairness

Our results verified that synthetic image generation can serve as test data for evaluating the fairness of pre-trained models. For instance, when examining the performance of pre-trained models, we confirm that for sex and skin type, *MelaNet* shows the most fair behavior, with  $\Delta_{\text{TPR}}$  of 0.0115 and 0.1322. For age *SkinLesionDensnet* performs the best with 0.0682. Although we have managed to measure  $\Delta_{\text{TPR}}$  for model fairness comparison, we still lack a method for discovering the causes or factors of unfairness. Hence, the next step is to apply concept-based fairness [37, 42, 55] evaluation to understand the actual cause of the fairness issue.

## 5.4. Various Diagnoses for Testing

We focused on TPR assessed through the disparity in true positive rates ( $\Delta_{\text{TPR}}$ ) under a melanoma-only (positive) test design. To broaden the scope of fairness evaluation, we aim to extend the generator and evaluation protocol to multiple diagnostic categories (e.g., benign nevi and other lesion types) and to multi-class classifiers in the future. This will enable (i) analysis of misclassification patterns (false positives and false negatives) by PII group, (ii) computation of additional group fairness criteria beyond  $\Delta_{\text{TPR}}$ , such as equalized odds [19], and (iii) reporting of worst-group and macro-averaged metrics in the multi-class setting.

## 5.5. Synthetic Data for Facilitating Fair Models

In this study, we verified whether synthetic data can be used for AI model fairness testing. We found that our generated and synthetic images exhibit a similar trend in fairness prediction. The next step is to use synthetic images to train the model fairly by providing a balanced dataset. Thus, we plan to use the synthetic images for fair model implementation in the future.

## 6. Clinical Relevance Statement

Our work addresses the risk that AI-based melanoma classifiers perform unevenly across sex, age, and skin type because current dermoscopic datasets are demographically imbalanced. In contrast, the current standard treatment involves examination by a dermatologist and dermoscopy testing, with teledermatology and simple AI tools sometimes used as supplementary measures. Our controllable diffusion model generates demographically balanced synthetic melanoma cohorts and uses them to measure true-positive-rate disparities, enabling systematic, privacy-preserving fairness audits that are difficult with real data alone. For clinical use, the generator must be trained on representative data, coupled with automated and expert image quality control, and validated prospectively to show that synthetic-cohort fairness patterns predict disparities in real patients without reducing accuracy. Key risks include poor modeling of rare phenotypes, amplification of hidden data biases, distribution shifts between synthetic and clinical images, and over-reliance on synthetic audits in place of multi-center trials.

## 7. Conclusion

In this work, we trained a state-of-the-art generative model for controllable synthetic melanoma test image generation. We verified that synthetic images can serve as test data for evaluating the fairness of pre-trained models. We also found that performance declines modestly when the classifier and the generator are trained on disjoint datasets, underscoring the impact of dataset shift. This means that a strictly privacy-preserving, PII-free fairness audit is most reliable when both the generator and the detector originate from the same data distribution. Beyond fairness assessment, the synthetic test set proved helpful for stress-testing model robustness, suggesting that data-driven generation can serve as a general diagnostic tool for AI in medical imaging.

## Acknowledgements

Anonymized for the review process.

## References

- [1] Aayushman, Hemanth Gaddey, Vidhi Mittal, Manisha Chawla, and Gagan Raj Gupta. Fair and accurate skin disease image classification by alignment with clinical labels. In *International Conference on Medical Image Computing and Computer-Assisted Intervention*, pages 394–404. Springer, 2024. 2
- [2] Faizanuddin Ansari, Tapabrata Chakraborti, and Swagatam Das. Algorithmic fairness in lesion classification by mitigating class imbalance and skin tone bias. In *International Conference on Medical Image Computing and Computer-Assisted Intervention*, pages 373–382. Springer, 2024. 2
- [3] Melina Arnold, Deependra Singh, Mathieu Laversanne, Jerome Vignat, Salvatore Vaccarella, Filip Meheus, Anne E Cust, Esther De Vries, David C Whiteman, and Freddie Bray. Global burden of cutaneous melanoma in 2020 and projections to 2040. *JAMA dermatology*, 158(5):495–503, 2022. 1
- [4] Christoph Baur, Shadi Albarqouni, and Nassir Navab. Melanogans: High resolution skin lesion synthesis with gans. *arXiv preprint arXiv:1804.04338*, 2018. 2
- [5] Peter J Bevan and Amir Atapour-Abarghouei. Detecting melanoma fairly: Skin tone detection and debiasing for skin lesion classification. In *MICCAI Workshop on Domain Adaptation and Representation Transfer*, pages 1–11. Springer, 2022. 2
- [6] Yequan Bie, Luyang Luo, Zhixuan Chen, and Hao Chen. Xcoop: Explainable prompt learning for computer-aided diagnosis via concept-guided context optimization. In *International Conference on Medical Image Computing and Computer-Assisted Intervention*, pages 773–783. Springer, 2024. 2
- [7] Alceu Bissoto, Fábio Perez, Eduardo Valle, and Sandra Avila. Skin lesion synthesis with generative adversarial networks. *arXiv preprint arXiv:1902.03253*, 2019. 2
- [8] Sandra Carrasco Limeros, Sylwia Majchrowska, Mohamad Khir Zoubi, Anna Rosén, Juulia Suvilehto, Lisa Sjöblom, and Magnus Kjellberg. Assessing gan-based generative modeling on skin lesions images. In *Machine Intelligence and Digital Interaction Conference*, pages 93–102. Springer Nature Switzerland Cham, 2022. 2
- [9] Elizabeth Chao, Chelsea K Meenan, and Laura K Ferris. Smartphone-based applications for skin monitoring and melanoma detection. *Dermatologic clinics*, 35(4):551–557, 2017. 1
- [10] Noel Codella, Veronica Rotemberg, Philipp Tschandl, M Emre Celebi, Stephen Dusza, David Gutman, Brian Helba, Aadi Kaloo, Konstantinos Liopyris, Michael Marchetti, et al. Skin lesion analysis toward melanoma detection 2018: A challenge hosted by the international skin imaging collaboration (isic). *arXiv preprint arXiv:1902.03368*, 2019. 2
- [11] Noel CF Codella, David Gutman, M Emre Celebi, Brian Helba, Michael A Marchetti, Stephen W Dusza, Aadi Kaloo, Konstantinos Liopyris, Nabin Mishra, Harald Kittler, et al. Skin lesion analysis toward melanoma detection: A challenge at the 2017 international symposium on biomedical imaging (isbi), hosted by the international skin imaging collaboration (isic). In *2018 IEEE 15th international symposium on biomedical imaging (ISBI 2018)*, pages 168–172. IEEE, 2018. 2
- [12] David Dembinsky, Adriano Lucieri, Stanislav Frolov, Hiba Najjar, Ko Watanabe, and Andreas Dengel. Unifying vxai: A systematic review and framework for the evaluation of explainable ai. *arXiv preprint arXiv:2506.15408*, 2025. 2
- [13] Emily L Denton, Soumith Chintala, Rob Fergus, et al. Deep generative image models using a laplacian pyramid of adversarial networks. *Advances in neural information processing systems*, 28, 2015. 2
- [14] European Union High-Level Expert Group on AI. Ethics guidelines for trustworthy ai, 2019. 2
- [15] Nils Gessert, Thilo Sentker, Frederic Madesta, Rüdiger Schmitz, Helge Kniep, Ivo Baltruschat, René Werner, and Alexander Schlaefer. Skin lesion classification using cnns with patch-based attention and diagnosis-guided loss weighting. *IEEE Transactions on Biomedical Engineering*, 67(2):495–503, 2020. 2, 3
- [16] Amirata Ghorbani, Vivek Natarajan, David Coz, and Yuan Liu. Dermgan: Synthetic generation of clinical skin images with pathology. *arXiv preprint arXiv:1911.08716*, 2019. 2
- [17] Ian Goodfellow, Jean Pouget-Abadie, Mehdi Mirza, Bing Xu, David Warde-Farley, Sherjil Ozair, Aaron Courville, and Yoshua Bengio. Generative adversarial networks. *Communications of the ACM*, 63(11):139–144, 2020. 2
- [18] David Gutman, Noel CF Codella, Emre Celebi, Brian Helba, Michael Marchetti, Nabin Mishra, and Allan Halpern. Skin lesion analysis toward melanoma detection: A challenge at the international symposium on biomedical imaging (isbi) 2016, hosted by the international skin imaging collaboration (isic). *arXiv preprint arXiv:1605.01397*, 2016. 2
- [19] Moritz Hardt, Eric Price, and Nathan Srebro. Equality of opportunity in supervised learning. In *Proceedings of the 30th International Conference on Neural Information Processing Systems*, page 3323–3331, Red Hook, NY, USA, 2016. Curran Associates Inc. 3, 8
- [20] Kaiming He, Xinlei Chen, Saining Xie, Yanghao Li, Piotr Dollár, and Ross Girshick. Masked autoencoders are scalable vision learners. In *Proceedings of the IEEE/CVF conference on computer vision and pattern recognition*, pages 16000–16009, 2022. 3
- [21] Carlos Hernández-Pérez, Marc Combalia, Sebastian Podlipnik, Noel CF Codella, Veronica Rotemberg, Allan C Halpern, Ofer Reiter, Cristina Carrera, Alicia Barreiro, Brian Helba, et al. Bcn20000: Dermoscopic lesions in the wild. *Scientific data*, 11(1):641, 2024. 2
- [22] Jonathan Ho, Ajay Jain, and Pieter Abbeel. Denoising diffusion probabilistic models. *Advances in neural information processing systems*, 33:6840–6851, 2020. 2
- [23] Thorsten Kalb, Kaisar Kushibar, Celia Cintas, Karim Lekadir, Oliver Diaz, and Richard Osuala. Revisiting skin tone fairness in dermatological lesion classification. In *Workshop on Clinical Image-Based Procedures*, pages 246–255. Springer, 2023. 4

- [24] Tero Karras, Samuli Laine, and Timo Aila. A style-based generator architecture for generative adversarial networks. In *Proceedings of the IEEE/CVF conference on computer vision and pattern recognition*, pages 4401–4410, 2019. 2
- [25] Tero Karras, Miika Aittala, Janne Hellsten, Samuli Laine, Jaakko Lehtinen, and Timo Aila. Training generative adversarial networks with limited data. *Advances in neural information processing systems*, 33:12104–12114, 2020. 2
- [26] Alexander Katalinic, Annika Waldmann, Martin A Weinstock, Alan C Geller, Nora Eisemann, Ruediger Greinert, Beate Volkmer, and Eckhard Breitbart. Does skin cancer screening save lives? an observational study comparing trends in melanoma mortality in regions with and without screening. *Cancer*, 118(21):5395–5402, 2012. 1
- [27] Jeremy Kawahara, Sara Daneshvar, Giuseppe Argenziano, and Ghassan Hamarneh. Seven-point checklist and skin lesion classification using multitask multimodal neural nets. *IEEE journal of biomedical and health informatics*, 23(2):538–546, 2018. 2
- [28] Diederik P Kingma and Max Welling. Auto-encoding variational bayes. *arXiv preprint arXiv:1312.6114*, 2013. 3
- [29] Newton M. Kinyanjui, Timothy Odonga, Celia Cintas, Noel C. F. Codella, Rameswar Panda, Prasanna Sattigeri, and Kush R. Varshney. Fairness of classifiers across skin tones in dermatology. In *Medical Image Computing and Computer Assisted Intervention – MICCAI 2020: 23rd International Conference, Lima, Peru, October 4–8, 2020, Proceedings, Part VI*, page 320–329, Berlin, Heidelberg, 2020. Springer-Verlag. 4
- [30] Young Joon Kwon, Danielle Toussie, Lea Azour, Jose Concepcion, Corey Eber, G. Anthony Reina, Ping Tak Peter Tang, Amish H. Doshi, Eric K. Oermann, and Anthony B. Costa. Appropriate evaluation of diagnostic utility of machine learning algorithm generated images. In *Proceedings of the Machine Learning for Health NeurIPS Workshop*, pages 179–193. PMLR, 2020. 8
- [31] Xiaoxiao Li, Ziteng Cui, Yifan Wu, Lin Gu, and Tatsuya Harada. Estimating and improving fairness with adversarial learning. *arXiv preprint arXiv:2103.04243*, 2021. 4
- [32] Ilya Loshchilov and Frank Hutter. Decoupled weight decay regularization. *International Conference on Learning Representations (ICLR)*, 2019. 3
- [33] Adriano Lucieri, Muhammad Naseer Bajwa, Stephan Alexander Braun, Muhammad Imran Malik, Andreas Dengel, and Sheraz Ahmed. Exaid: A multimodal explanation framework for computer-aided diagnosis of skin lesions. *Computer Methods and Programs in Biomedicine*, 215:106620, 2022. 1
- [34] Xiaopu Ma, Jiangdan Shan, Fei Ning, Wentao Li, and He Li. Effnet: A skin cancer classification model based on feature fusion and random forests. *Plos one*, 18(10): e0293266, 2023. 2, 3
- [35] Mayur Mallya and Ghassan Hamarneh. Deep multimodal guidance for medical image classification. In *International Conference on Medical Image Computing and Computer-Assisted Intervention*, pages 298–308. Springer, 2022. 2, 3, 4
- [36] MILK Study Team. Milk10k. ISIC Archive, 2025. 1
- [37] Isar Nejadgholi, Esma Balkir, Kathleen C Fraser, and Svetlana Kiritchenko. Towards procedural fairness: Uncovering biases in how a toxic language classifier uses sentiment information. In *Proceedings of the fifth Black-boxNLP workshop on analyzing and interpreting neural networks for NLP*, pages 225–237, 2022. 8
- [38] Maxime Oquab, Timothée Darcet, Théo Moutakanni, Huy Vo, Marc Szafraniec, Vasil Khalidov, Pierre Fernandez, Daniel Haziza, Francisco Massa, Alaaeldin El-Nouby, et al. Dinov2: Learning robust visual features without supervision. *arXiv preprint arXiv:2304.07193*, 2023. 3
- [39] Frederik Pahde, Maximilian Dreyer, Wojciech Samek, and Sebastian Lapuschkin. Reveal to revise: An explainable ai life cycle for iterative bias correction of deep models. In *International Conference on Medical Image Computing and Computer-Assisted Intervention*, pages 596–606. Springer, 2023. 2
- [40] Saswat Panda, Abhishek Sunil Tiwari, and Manas Ranjan Prusty. Comparative study on different deep learning models for skin lesion classification using transfer learning approach. *International Journal of Scientific and Research Publications*, 11(1):219–32, 2021. 2, 3, 4
- [41] William Peebles and Saining Xie. Scalable diffusion models with transformers. In *Proceedings of the IEEE/CVF international conference on computer vision*, pages 4195–4205, 2023. 2
- [42] Varsha Pendyala and Jihye Choi. Concept-based explanations for tabular data. *arXiv preprint arXiv:2209.05690*, 2022. 8
- [43] Alec Radford, Luke Metz, and Soumith Chintala. Unsupervised representation learning with deep convolutional generative adversarial networks. *arXiv preprint arXiv:1511.06434*, 2015. 2
- [44] Alec Radford, Jong Wook Kim, Luke Hallacy, Aditya Ramesh, Gabriel Goh, Sandhini Agarwal, Girish Sastry, Amanda Askell, Pamela Mishkin, Jack Clark, Gretchen Krueger, and Ilya Sutskever. Learning transferable visual models from natural language supervision. In *Proceedings of the 38th International Conference on Machine Learning (ICML)*, 2021. 3
- [45] Cédric Rat, Sandrine Hild, Julie Rault Sérandour, Aurélie Gaultier, Gaëlle Quereux, Brigitte Dreno, and Jean-Michel Nguyen. Use of smartphones for early detection of melanoma: systematic review. *Journal of medical Internet research*, 20(4):e135, 2018. 1
- [46] David Rolnick, Andreas Veit, Serge Belongie, and Nir Shavit. Deep learning is robust to massive label noise. *arXiv preprint arXiv:1705.10694*, 2017. 6
- [47] Robin Rombach, Andreas Blattmann, Dominik Lorenz, Patrick Esser, and Björn Ommer. High-resolution image synthesis with latent diffusion models. In *Proceedings of the IEEE/CVF conference on computer vision and pattern recognition*, pages 10684–10695, 2022. 2
- [48] Verónica Rotemberg, Nicholas Kurtansky, Brigid Betz-Stablein, Liam Caffery, Emmanouil Chousakos, Noel

- Codella, Marc Combalia, Stephen Dusza, Pascale Guitera, David Gutman, et al. A patient-centric dataset of images and metadata for identifying melanomas using clinical context. *Scientific data*, 8(1):34, 2021. 2
- [49] Nataniel Ruiz, Yuanzhen Li, Varun Jampani, Yael Pritch, Michael Rubinstein, and Kfir Aberman. Dreambooth: Fine tuning text-to-image diffusion models for subject-driven generation. In *Proceedings of the IEEE/CVF conference on computer vision and pattern recognition*, pages 22500–22510, 2023. 2
- [50] Rukhsar Sabir and Tahir Mehmood. Classification of melanoma skin cancer based on image data set using different neural networks. *Scientific Reports*, 14(1):29704, 2024. 3
- [51] Silonie Sachdeva. Fitzpatrick skin typing: Applications in dermatology. *Indian journal of dermatology, venereology and leprology*, 75:93, 2009. 2
- [52] Yi Sheng, Junhuan Yang, Jinyang Li, James Alaina, Xi-aowei Xu, Yiyu Shi, Jingtong Hu, Weiwen Jiang, and Lei Yang. Data-algorithm-architecture co-optimization for fair neural networks on skin lesion dataset. In *International Conference on Medical Image Computing and Computer-Assisted Intervention*, pages 153–163. Springer, 2024. 2
- [53] Emma A. M. Stanley, Matthias Wilms, and Nils D. Forkert. Disproportionate subgroup impacts and other challenges of fairness in artificial intelligence for medical image analysis. In *Ethical and Philosophical Issues in Medical Imaging, Multimodal Learning and Fusion Across Scales for Clinical Decision Support, and Topological Data Analysis for Biomedical Imaging: 1st International Workshop, EPIMI 2022, 12th International Workshop, ML-CDS 2022, 2nd International Workshop, TDA4BiomedicalImaging, Held in Conjunction with MIC-CAI 2022, Singapore, September 18–22, 2022, Proceedings*, page 14–25, Berlin, Heidelberg, 2022. Springer-Verlag. 4
- [54] Chi-en Amy Tai, Oustan Ding, and Alexander Wong. Cancer-net sca-synth: An open access synthetically generated 2d skin lesion dataset for skin cancer classification. *arXiv preprint arXiv:2411.05269*, 2024. 2
- [55] Schrasing Tong and Lalana Kagal. Investigating bias in image classification using model explanations. *arXiv preprint arXiv:2012.05463*, 2020. 4, 8
- [56] Philipp Tschandl, Cliff Rosendahl, and Harald Kittler. The ham10000 dataset, a large collection of multi-source dermatoscopic images of common pigmented skin lesions. *Scientific data*, 5(1):1–9, 2018. 2
- [57] Janet Wang, Yunsung Chung, Zhengming Ding, and Jihun Hamm. From majority to minority: A diffusion-based augmentation for underrepresented groups in skin lesion analysis. In *International Conference on Medical Image Computing and Computer-Assisted Intervention*, pages 14–23. Springer, 2024. 2
- [58] Caroline G Watts, Kirstie McLoughlin, Chris Goumas, Cathelijne H Van Kemenade, Joanne F Aitken, H Peter Soyer, Pablo Fernandez Peñas, Pascale Guitera, Richard A Scolyer, Rachael L Morton, et al. Association between melanoma detected during routine skin checks and mortality. *JAMA dermatology*, 157(12):1425–1436, 2021. 1
- [59] Jingfeng Yao, Bin Yang, and Xinggang Wang. Reconstruction vs. generation: Taming optimization dilemma in latent diffusion models. In *Proceedings of the Computer Vision and Pattern Recognition Conference*, pages 15703–15712, 2025. 2, 3, 4, 7
- [60] Jingyi Zhang, Jiaying Huang, Sheng Jin, and Shijian Lu. Vision-language models for vision tasks: A survey. *IEEE transactions on pattern analysis and machine intelligence*, 46(8):5625–5644, 2024. 8
- [61] Hasib Zunair and A Ben Hamza. Melanoma detection using adversarial training and deep transfer learning. *Physics in Medicine & Biology*, 2020. 2, 3, 4

# Supplementary Material:

## Towards Facilitated Fairness Assessment of AI-based Skin Lesion Classifiers Through GenAI-based Image Synthesis

Ko Watanabe\*

DFKI GmbH  
ko.watanabe@dfki.de

Stanislav Frolov\*

DFKI GmbH  
stanislav.frolov@dfki.de

Aya Hassan

RPTU Kaiserslautern-Landau  
aya.hassan@dfki.de

David Dembinsky

DFKI GmbH  
david.dembinsky@dfki.de

Adriano Lucieri

DFKI GmbH  
adriano.lucieri@dfki.de

Andreas Dengel

DFKI GmbH  
andreas.dengel@dfki.de

\*Equal contribution

### Analysis of sampling parameters

To better understand the performance of our generative model we sweep the classifier-free guidance (CFG) scale and number of sampling steps, see [Table 1](#). We find that the default sampling parameters are not optimal. Instead, a lower CFG and higher number of steps produce the best FID (lower is better). Therefore, we show synthetic images using these optimal parameters in the main paper. For comparison, we display synthetic images with default sampling parameters in [Figure 1](#).

### Impact of data availability on generation quality

Next, we are interested in the relationship between data availability and final generation quality. To that end, we measure the FID of synthetic images grouped by age against real data and compute the corresponding available training data for said age group in [Table 2](#). We find that the generation quality correlates well with the data availability. Specifically, the best FID is achieved for age group 50 and 60, both represented more than 10% in the training data.

### Visualization of real testing data

In [Figure 2](#), we visualize real testing data from the MILK10k [2] dataset. Firstly, we observe that many combinations are simply not available thus making fairness assessment challenging. Secondly, as seen in both the real and synthetic images, they do not become progressively darker with higher Fitzpatrick skin types. Prior work [1, 3] shows that this intuitive assumption fails because lighting, camera settings, and lesion visibility heavily affect perceived darkness, leading expert-, crowd-, and algorithm-based annotations to diverge. Due to this variability, raw pixel intensity is an unreliable indicator of skin type, and higher categories do not consistently appear darker, highlighting the need for calibrated annotations rather than appearance alone.

### Nearest neighbours visualization

To further assess the capabilities of our generative model, we visualize synthetic images alongside their real nearest neighbours from the training set in [Figure 3–Figure 6](#). The generated samples are highly realistic yet clearly distinct from their nearest neighbours, indicating that the model does not merely memorize the training data.

### Zero-shot classification comparison

Finally, we are interested in the performance of WhyLesionCLIP [4], a fine-tuned version of OpenCLIP, on real as well as our synthetic images, see [Figure 7](#) to [Figure 13](#). WhyLesionCLIP [4] captures dermatological and clinical

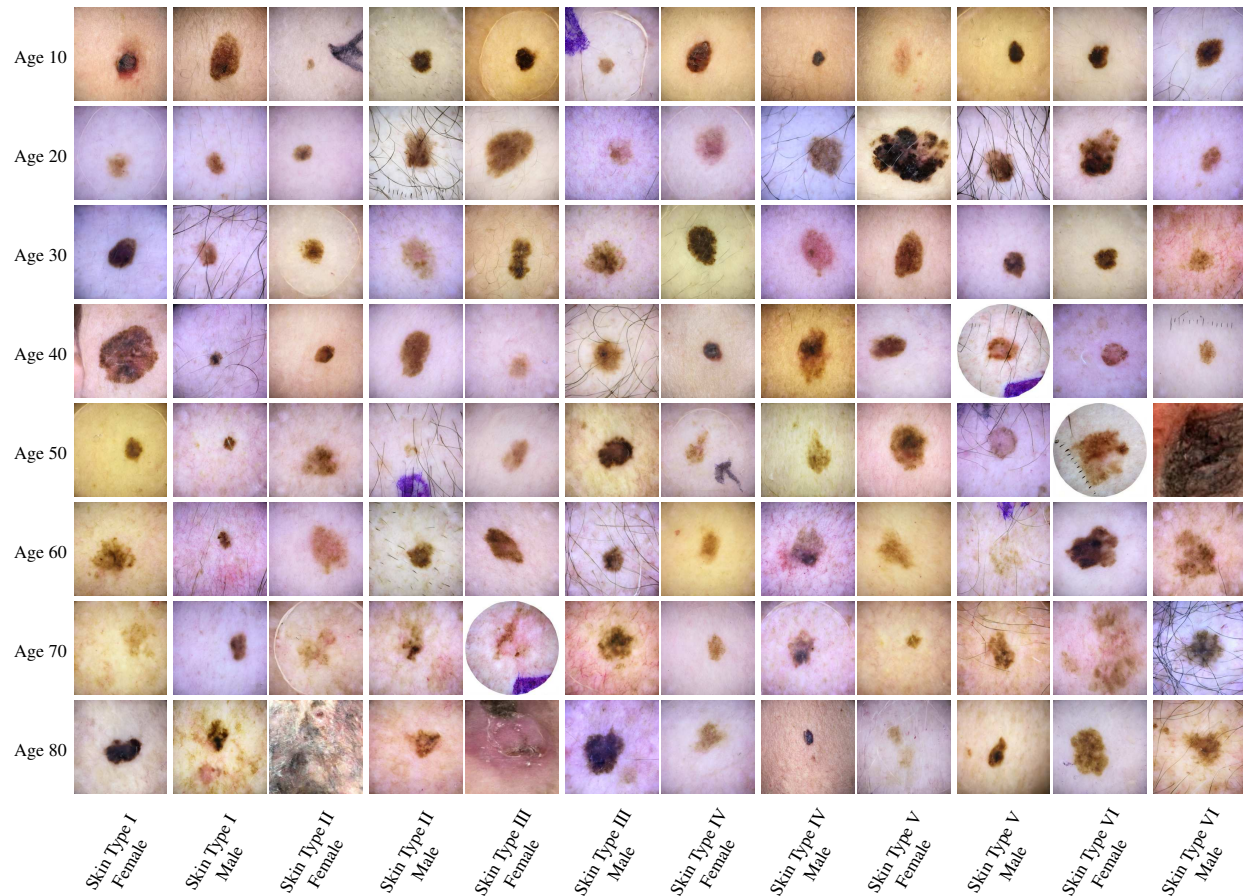


Figure 1. Synthetic melanoma images generated by our model with default sampling parameters (cfg=8, steps=200). Rows represent Fitzpatrick skin types (I–VI) combined with sex, and columns represent age groups (10–80). The grid demonstrates coverage of diverse demographic groups for fairness assessment.

semantics more reliably than general purpose CLIP models and is thus a good choice for general assessment. The zero-shot predictions were obtained using three prompt families corresponding to age, sex, and Fitzpatrick skin type. Age prompts covered the eight age groups and followed the template “A clinical close-up photograph of the {body\_site} skin of a {age}-year-old melanoma patient.” Sex prompts described the patient’s sex using the format “A clinical close-up photograph of the {body\_site} skin of a {sex} melanoma patient.” Fitzpatrick skin type prompts covered types I through VI using the template “A clinical close-up of the skin of a melanoma patient with Fitzpatrick type {type} ({description of the skin type}).” Overall, our synthetic images follow similar performance pattern across the age-sex-skin attributes, but our synthetic images are more recognizable as indicated by higher accuracies for all attribute groups. Interestingly, the performance across age groups is very imbalanced and varies a lot between real and synthetic showing that recognizing age from skin lesion images alone is difficult. Furthermore, both real and synthetic images are highly imbalances w.r.t to sex classification. Male accuracy is significantly lower than female accuracy, but our synthetic images are much better than real ones while reaching comparable performance for female. In terms of skin type classification, our synthetic images reach higher performance on all but skin type I, which is the best in real data. Finally, we visualize the CLIP score distributions by age, sex and skin type. Our synthetic images consistently lead to smoother distributions with higher mean values indicating better recognizability.

## References

- [1] Thorsten Kalb, Kaisar Kushibar, Celia Cintas, Karim Lekadir, Oliver Diaz, and Richard Osuala. Revisiting skin tone fairness in dermatological lesion classification. In *Workshop on Clinical Image-Based Procedures*, pages 246–255. Springer, 2023. 1

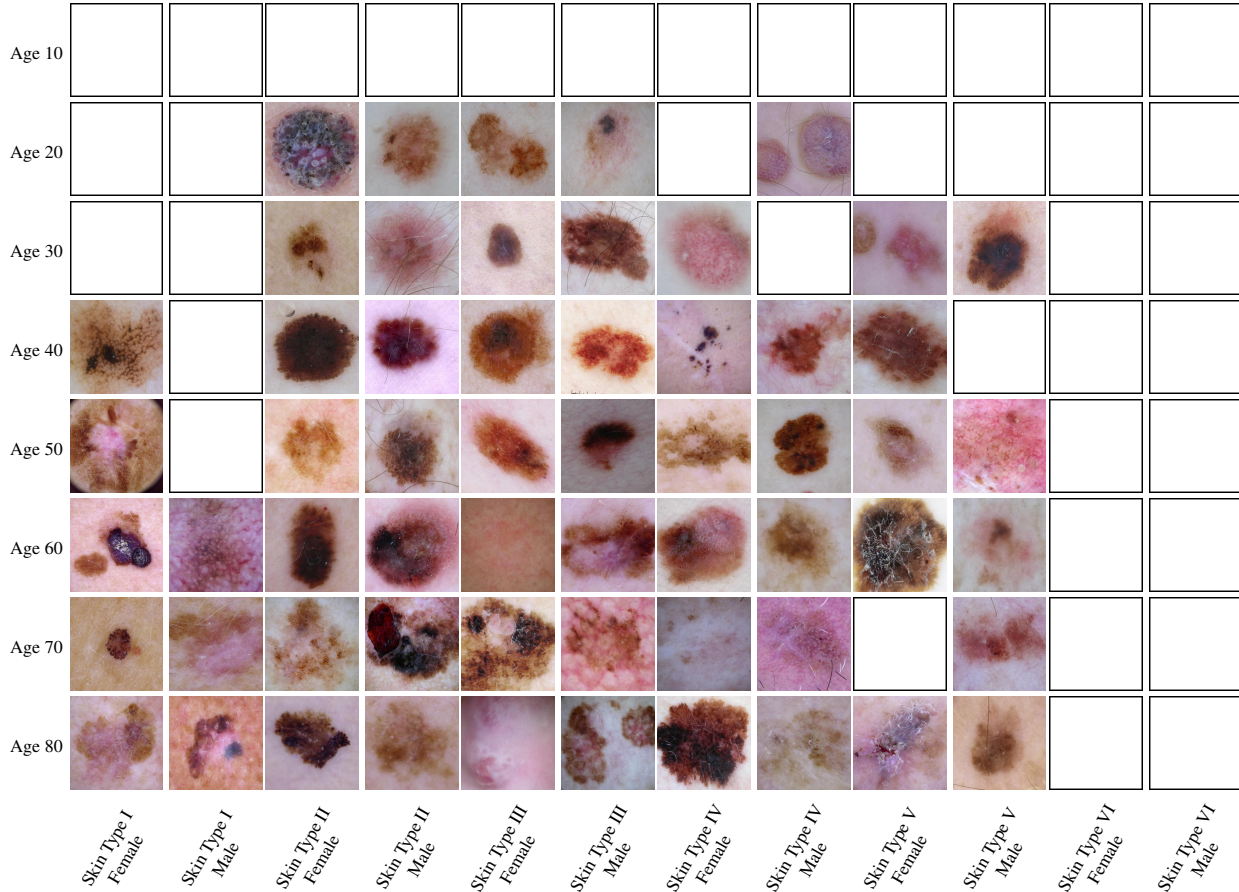


Figure 2. Real melanoma images from the MILK10k dataset [2]. Rows represent Fitzpatrick skin types (I–VI) combined with sex, and columns represent age groups (10–80). The grid demonstrates coverage of diverse demographic groups for fairness assessment. Many age–skin–sex combinations are missing from the real dataset, making fairness assessment difficult.

| cfg \ steps | 100   | 150   | 200          | 250   | 300   | 400          |
|-------------|-------|-------|--------------|-------|-------|--------------|
| 4.0         | 29.69 | 28.64 | 28.23        | 32.55 | 27.93 | <b>27.77</b> |
| 6.7         | 30.66 | 30.00 | 29.75        | 32.37 | 29.61 | 29.57        |
| 8.0         | 31.59 | 30.92 | <u>30.75</u> | 32.57 | 30.71 | 30.73        |
| 10.0        | 32.53 | 32.34 | 32.38        | 34.15 | 32.47 | 32.52        |
| 12.0        | 34.38 | 34.42 | 34.50        | 34.14 | 34.79 | 34.90        |

Table 1. FID averaged over age groups for each combination of classifier-free guidance (cfg) and diffusion steps showing that default setting (underlined) are not optimal settings (bold) when trained on skin lesions.

| Age | Mean FID     | Data ratio |
|-----|--------------|------------|
| 10  | 40.56        | 0.35%      |
| 20  | 36.88        | 0.66%      |
| 30  | 36.05        | 3.13%      |
| 40  | 30.84        | 8.06%      |
| 50  | 26.08        | 11.57%     |
| 60  | <b>25.74</b> | 12.50%     |
| 70  | 27.60        | 9.37%      |
| 80  | 28.94        | 5.00%      |

Table 2. Data ratio and mean FID over all cfg and steps for each age group. Generation quality generally correlates with the available training data.

[2] MILK Study Team. Milk10k. ISIC Archive, 2025. 1, 3

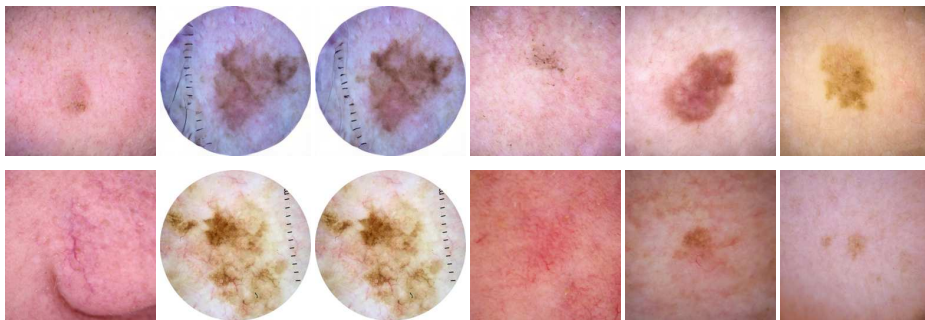
[3] Schrasing Tong and Lalana Kagal. Investigating bias in image classification using model explanations. *arXiv preprint arXiv:2012.05463*, 2020. 1

[4] Yue Yang, Mona Gandhi, Yufei Wang, Yifan Wu, Michael S. Yao, Chris Callison-Burch, James C. Gee, and Mark Yatskar. A textbook remedy for domain shifts: Knowledge priors for medical image analysis. *arXiv preprint arXiv:2405.14839*, 2024. 1

Age 10, Female



Age 10, Male



Age 20, Female



Age 20, Male

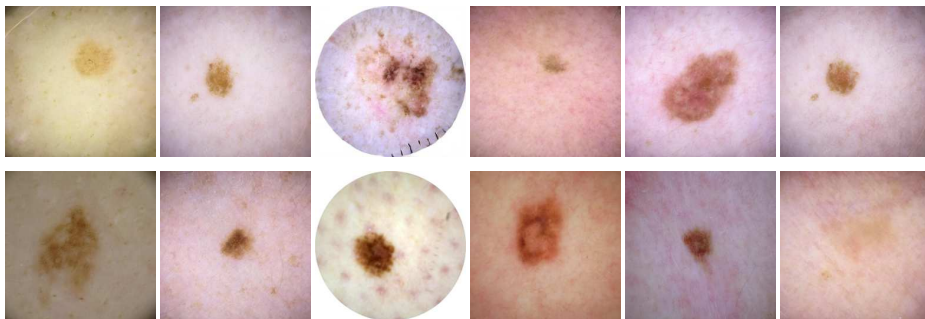


Figure 3. Synthetic samples (top row in each block) and nearest real neighbours (bottom row) for ages 10 and 20. Columns represent skin type I to VI.

Age 30, Female



Age 30, Male



Age 40, Female



Age 40, Male

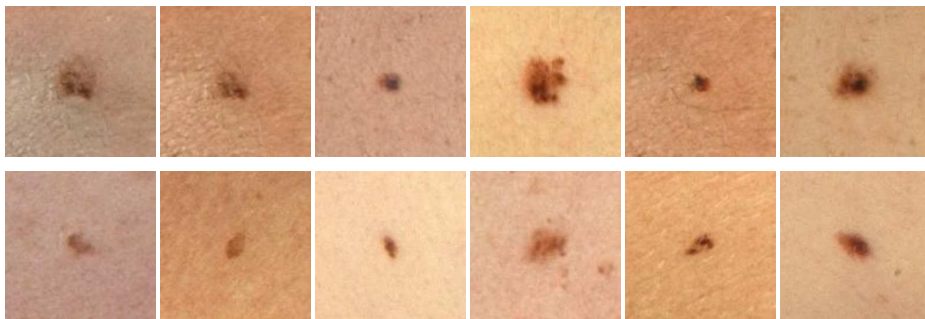


Figure 4. Synthetic samples (top row in each block) and nearest real neighbours (bottom row) for ages 30 and 40. Columns represent skin type I to VI.

Age 50, Female



Age 50, Male



Age 60, Female



Age 60, Male



Figure 5. Synthetic samples (top row in each block) and nearest real neighbours (bottom row) for ages 50 and 60. Columns represent skin type I to VI.

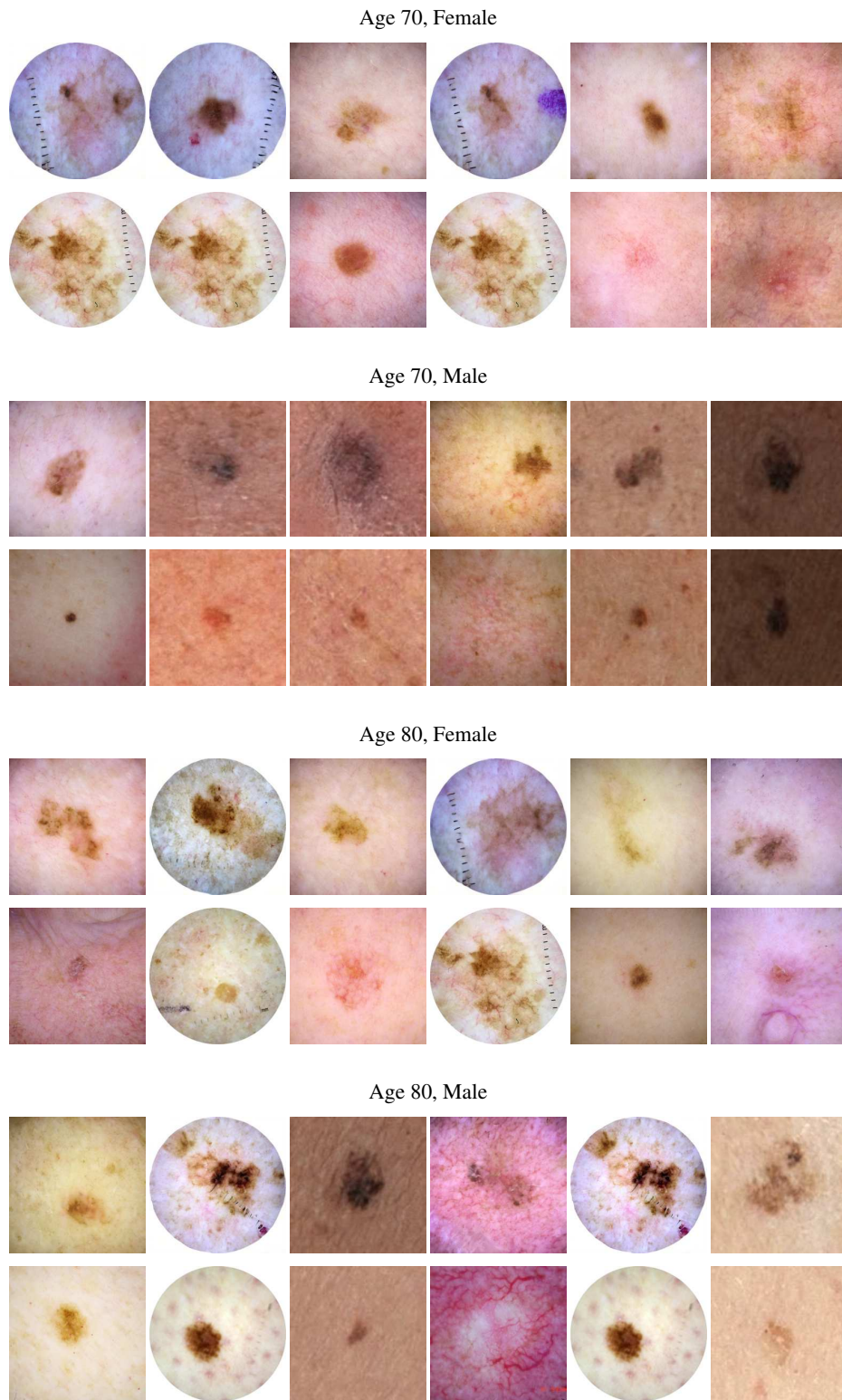
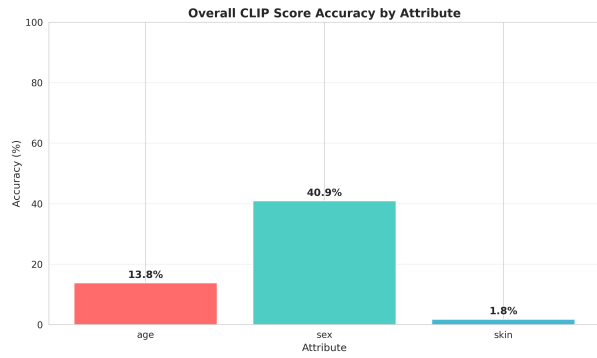
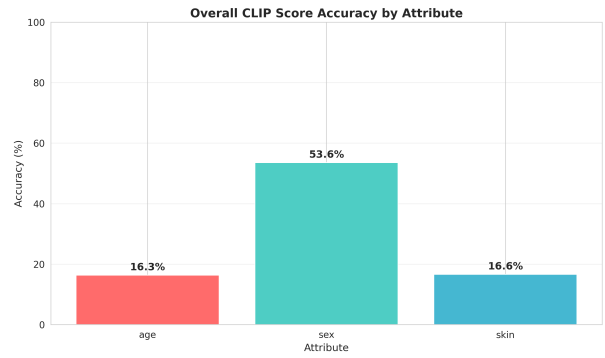


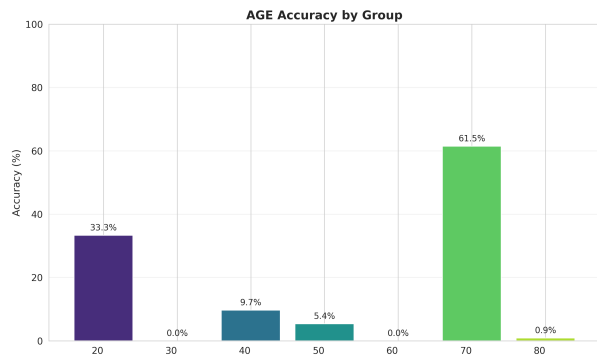
Figure 6. Synthetic samples (top row in each block) and nearest real neighbours (bottom row) for ages 70 and 80. Columns represent skin type I to VI.



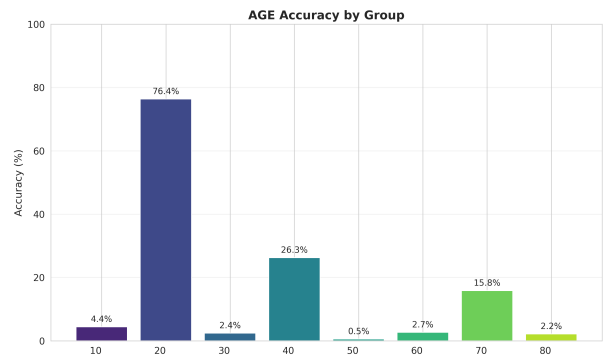
(a) Overall CLIP Score Accuracy (real)



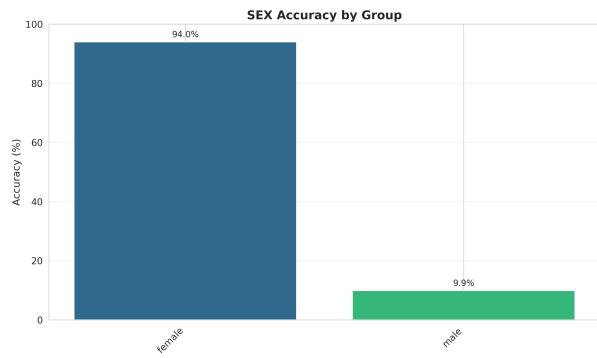
(b) Overall CLIP Score Accuracy (synthetic)



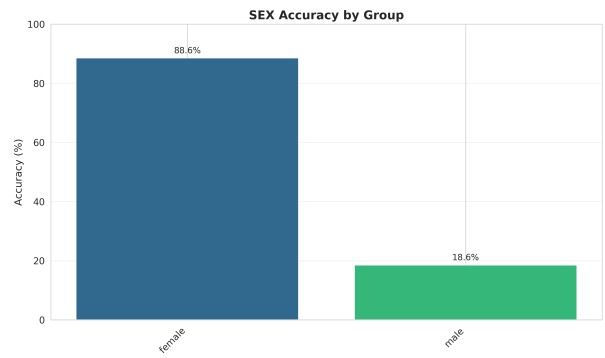
(c) AGE Accuracy (real)



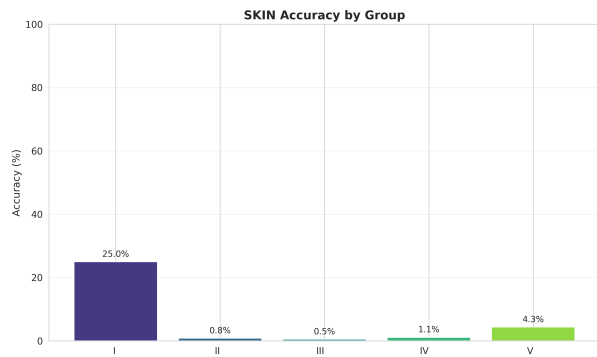
(d) AGE Accuracy (synthetic)



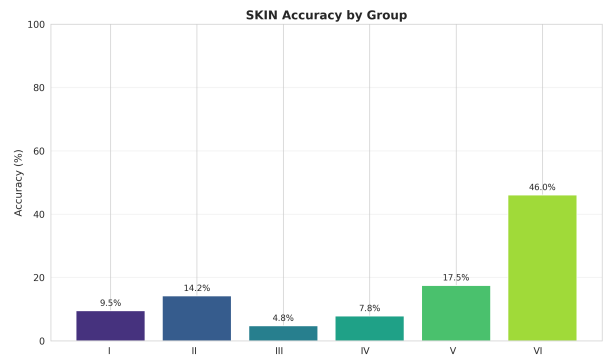
(e) SEX Accuracy (real)



(f) SEX Accuracy (synthetic)



(g) SKIN Accuracy (real)



(h) SKIN Accuracy (synthetic)

Figure 7. Comparison of CLIP-score classification accuracies across attributes.

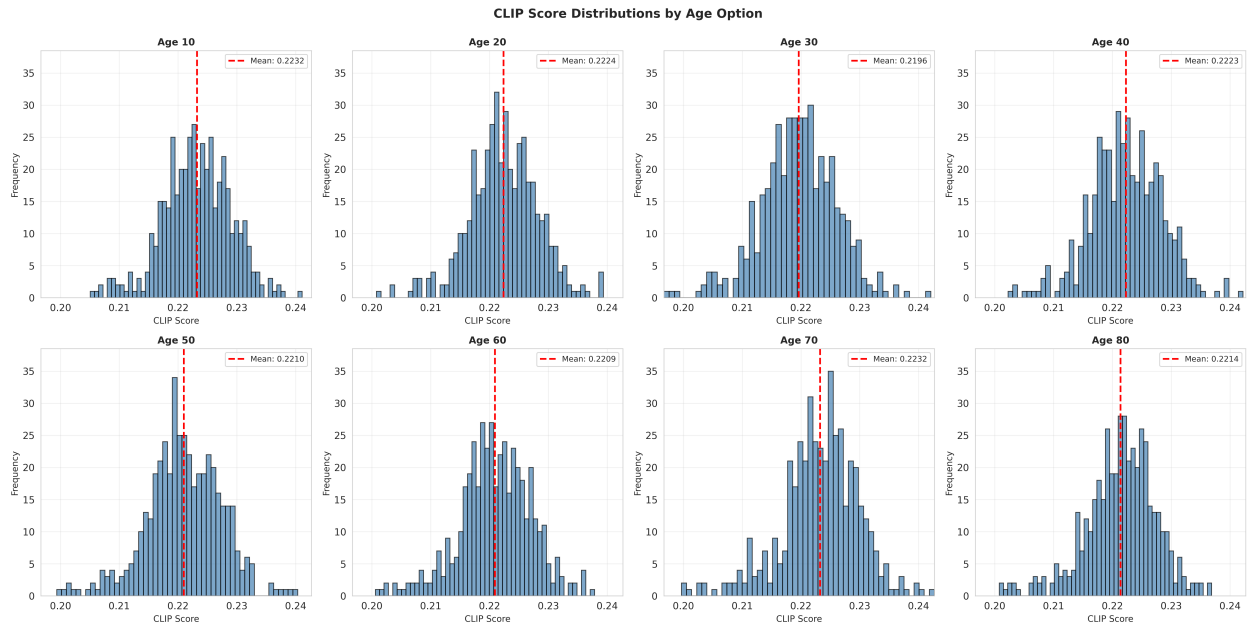


Figure 8. CLIP Score Distributions by Age (real)

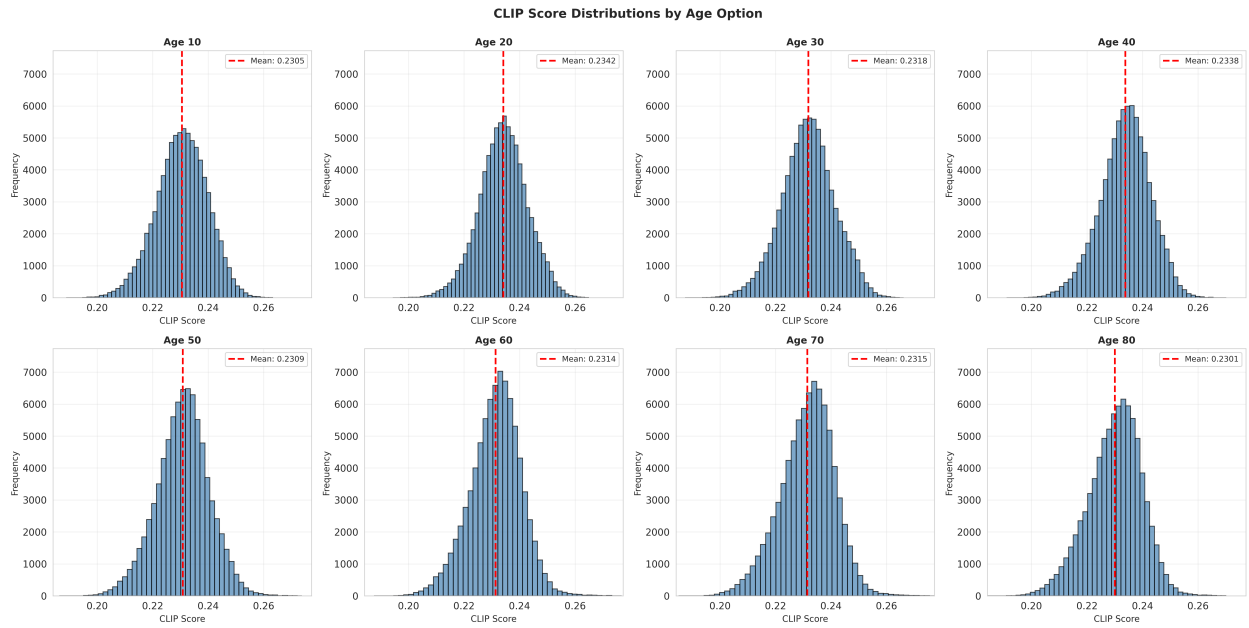


Figure 9. CLIP Score Distributions by Age (synthetic)

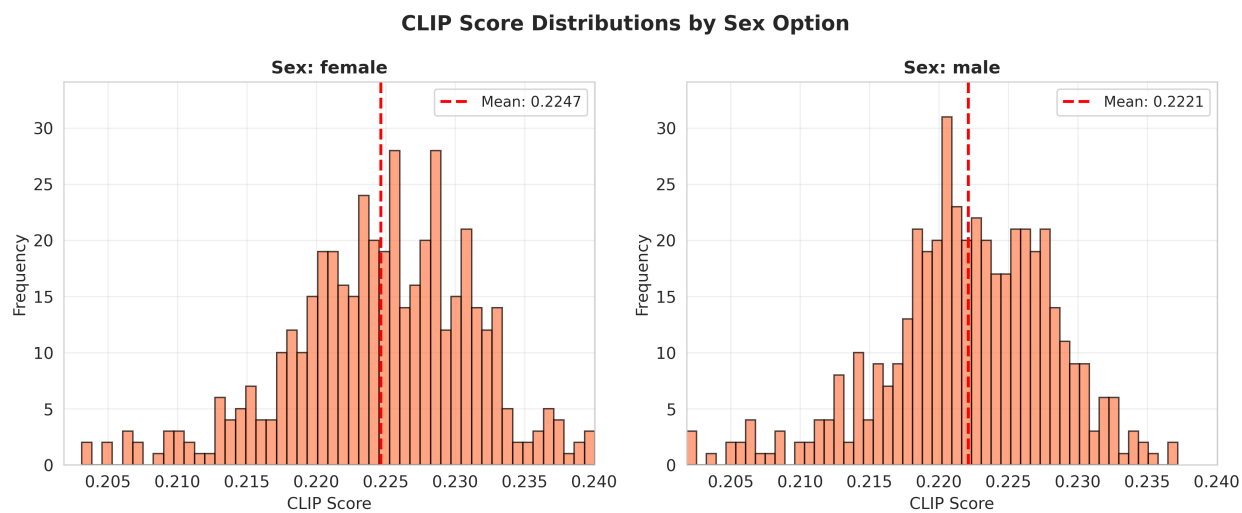


Figure 10. CLIP Score Distributions by Sex (real)

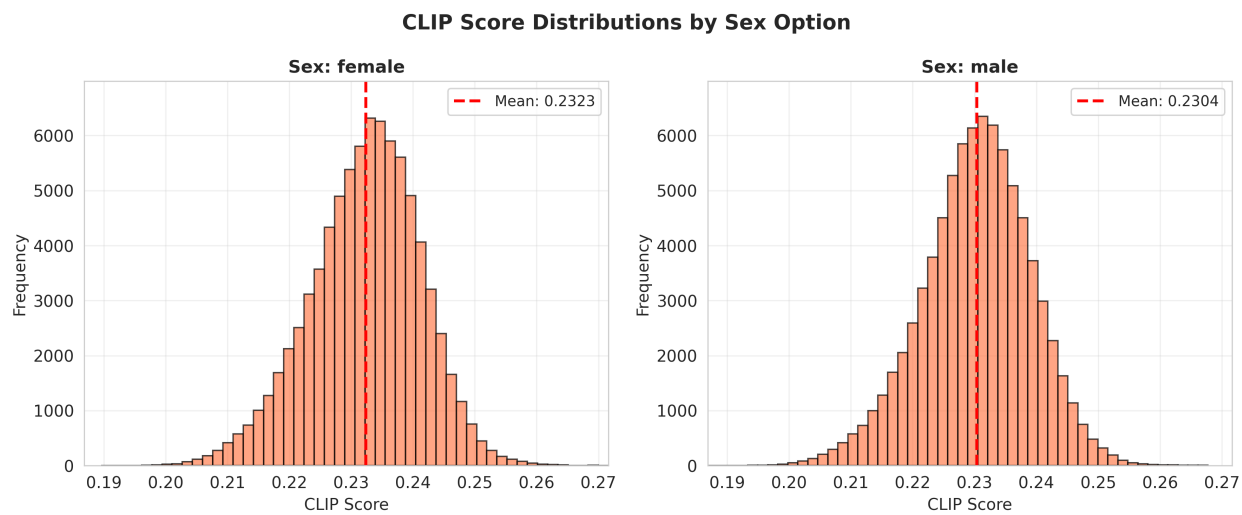


Figure 11. CLIP Score Distributions by Sex (synthetic)

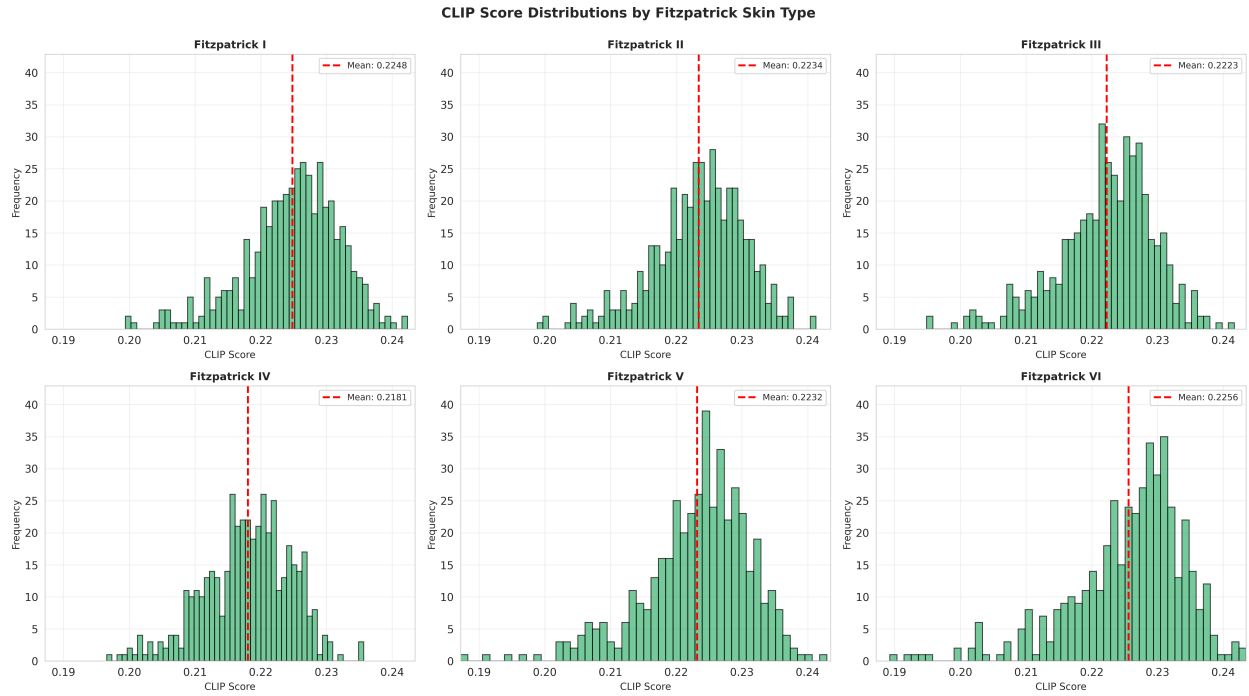


Figure 12. CLIP Score Distributions by Skin Type (real)

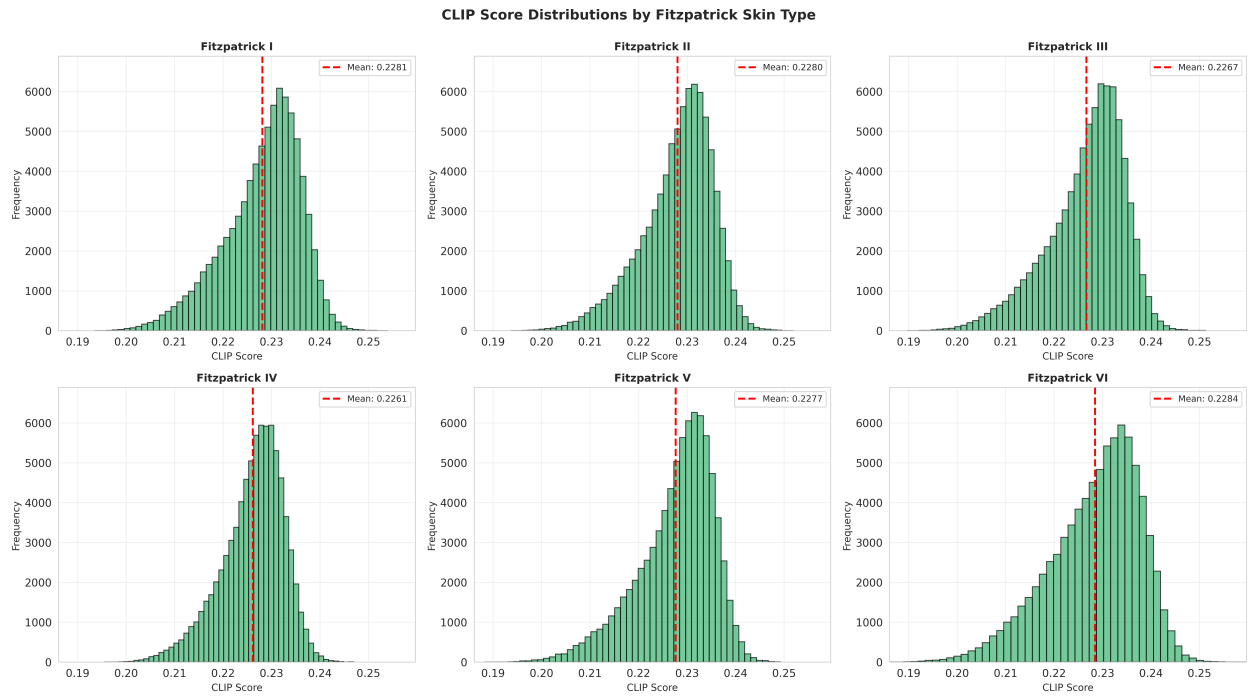


Figure 13. CLIP Score Distributions by Skin Type (synthetic)